ACADÉMIE
DES SCIENCES
INSTITUT DE FRANCE

Comptes Rendus
Chimie

Amenah Adnan Alfares, Afyaa Muayed Younis, Lana Abdalhameed Rasheed and Abdelrahman Basil Fadhil

Valorization of pinecone as a pyrolysis feedstock: identification of bio-oil and synthesis of activated biochar for Cr(VI) elimination from wastewater

Volume 27, Special Issue S3 (2024), p. 97-115

Online since: 27 November 2024

Part of Special Issue: Materials and Energy Valorization of Biomass and Waste: The Path for Sustainability and Circular Economy Promotion

Guest editors: Mejdi Jeguirim (Université de Haute-Alsace, Institut de Sciences des Matériaux de Mulhouse, France) and Salah Jellali (Sultan Qaboos University, Oman)

https://doi.org/10.5802/crchim.351

The Comptes Rendus. Chimie *are a member of the Mersenne Center for open scientific publishing*
www.centre-mersenne.org — e-ISSN : 1878-1543

ACADÉMIE DES SCIENCES
INSTITUT DE FRANCE

Comptes Rendus. Chimie
2024, Vol. 27, Special issue S3, p. 97-115
https://doi.org/10.5802/crchim.351

Research article

Materials and Energy Valorization of Biomass and Waste: The Path for Sustainability and Circular Economy Promotion

Valorization of pinecone as a pyrolysis feedstock: identification of bio-oil and synthesis of activated biochar for Cr(VI) elimination from wastewater

Amenah Adnan Alfares [a], Afyaa Muayed Younis [a], Lana Abdalhameed Rasheed [a] and Abdelrahman Basil Fadhil [a,*]

[a] Mosul University, Department of Chemistry, College of Science, Majmoaa Street, 41002, Mosul, Iraq

E-mails: amenahadnan@uomosul.edu.iq (A. A. Alfares), afyaamy2005@uomosul.edu.iq (A. M. Younis), lanaabdalhameed@uomosul.edu.iq (L. A. Rasheed), abdelrahmanbasil@yahoo.com, abdelrahmanbasil@uomosul.edu.iq (A. B. Fadhil)

Abstract. The thermal pyrolysis of pinecone (PC) to produce pyrolytic oil (PO) and solid biochar (BC) in a batch-scale fixed-bed reactor at numerous temperatures (400–600 °C) for diverse time intervals (30–120 min) using different particle sizes (0.26–0.841 mm) and various rates of heating (10–50 °C/min), as established in this work, led to the production of a high yield of the PO (42.12%) at 500 °C for 1 h with a 0.40 mm particle size and a heating rate of 30 °C/min. The bio-oil (BO) content in the resulting PO amounted to 10.20%. The ^{1}H NMR and GC-MS spectroscopy, besides the ultimate analysis of the BO, were identified. The consequences disclosed that the BO principally consisted of oxygenated hydrocarbons, which amounted to 54.98%, besides the N-organic compounds and hydrocarbons, whose contents were 6.95% and 2.60%, respectively. The BO had a high content of C and H besides its remarkably high caloric value (26.99 MJ/kg), suggesting its potential as a high-energy fuel. The K_2CO_3-activation of the BC leftover after the pyrolysis of PC produced a microporous activated biochar (ABC) with a BET surface area of 465.55 m^2/g and 1.97 nm average pore diameter using 2:1 K_2CO_3:BC impregnation ratio at 750 °C for 1 h. The ABC exhibited an adsorptive elimination of 98.71% for 100 mL of solution containing 150 ppm of Cr(VI) from its aqueous phase using 0.20 g of ABC at 35 °C for 140 min and a pH = 2.0. The Langmuir isotherm and the psedue-2nd-order model of kinetics best described the Cr(VI) adsorption by the ABC. In conclusion, PC could be used as a pyrolysis feedstock to produce BO with high-content aromatic oxygenates besides ABC with a high surface area, a microporous structure and an efficient ability to eliminate Cr(VI) ions from wastewater.

Keywords. Pinecone, Pyrolysis, Bio-oil, Activated biochar, Cr(VI) adsorption.

Manuscript received 11 April 2024, revised 16 July 2024 and 3 September 2024, accepted 1 October 2024.

* Corresponding author

1. Introduction

Due to the growing awareness of environmental protection and the diminishing of petroleum reserves, the search for renewable and eco-friendly resources has gained prominence [1–4]. Biomass (BM) is a significant alternative energy source that can slow down the fossil fuels depletion. The BM-based precursors are renewable, and producing biofuel from such sources via thermal pyrolysis is a promising approach to converting BM into numerous products compared to other thermochemical conversion processes [5,6]. In this technique, the BM precursor is heated in the presence or absence of a catalyst to create various energy sources (liquid, gas, or solid) in a temperature range between 450–600 °C in a limited oxygen environment [4]. Fast pyrolysis is the most common method of converting BM feed into a liquid fuel called PO or BO. Nonetheless, the latter owns several defects in handling, storage, and transportation besides having several merits compared with solid sources [5]. One of the typical uses of the PO is as an alternative fuel for furnaces [6]. However, its usage in engines and turbines requires some modification, including reducing its elevated content of O-compounds [6,7]. The PO can also be employed in synthesizing bio-chemicals through catalytic pyrolysis [6,7].

Numerous studies have been announced in the literature on the thermal pyrolysis of varied biowastes and non-edible seeds to produce multiple pyrolysis products, including PO and biochar (BC). Table 1 offers pyrolysis conditions required to produce the desired products from multiple BM feeds in the literature. According to Table 1, it is notable that the products yield from the thermal pyrolysis of various BM precursors can be attributed to many factors, including the chemical composition of the parent feed viz. its content of cellulose, hemi cellulose and lignin, which their ratios in the authentic raw material affects greatly its pyrolysis products output [8].

As a member of the *Pinaceae* family, pines are perennial trees with an average height of 50 m. The pine trees carry dark green needles bearing cones. The cone is convex with a length of 5–10 cm. As an outcome of the massive production of cones worldwide, cones are discarded as solid waste (Figure 1). Most pine trees are mostly planted to be involved in the manufacture of paper pulps [21].

Like any BM material, the PC comprises cellulose, lignin, and resins. When the PC is subjected to thermal destruction, these constituents are decomposed to evolve multiple gaseous products, leaving behind a solid residue with a carbonaceous structure that could be a valuable precursor to synthesize activated carbon (AC) [22]. Cellulose, hemicellulose, lignin, and other constituents of PC comprise functional groups, including the sulfhydryl (thiol), carbonyl (ketone), alcohols, carboxyl, sulfonate, esters, thioether, and amine. Such functional groups can be helpful in linking to heavy metals [22]. According to the literature, PC was used in multi purposes. For example, Abujazar et al. [23] announced the utilization of PC powder as a cheap and natural coagulant agent for treating iron and steel factory effluents, and proved its effectiveness for this purpose. Guo et al. [24] synthesized sulfonated hydrochar to be employed as an effective catalyst for the dehydration of carbohydrate. Lastly, the integrated steam gasification process of PC for the production of H_2 and biomethanol was declared by Turgut and Dincer [25]. In addition to those studied, the utilization of PC as a potential precursor for AC synthesis was also announced in the literature. In general, the PC was transformed into BC, and the latter was modified and used as an adsorbent to eliminate bisphenol-A and a toxic azo dye (SB3) from aqueous medium with a removal capacity of 38.387 mg/g and 346.856 mg/g, respectively [26]. The BC resulting from the thermal destruction of PC was modified with $AlCl_3$, and the resulting composites were implemented in extracting F-ions from drinking groundwater with an elimination capacity of 14.07 mg/g and a removal performance of 87.13% [27]. Carbonization of PC to BC, followed by KOH-activation of the latter to synthesize AC for removing naphthalene from paraffin oil, was announced in the literature with a removal capacity of 435 mg/g [28]. A magnetic hydrochar was produced from PC and then treated with ammonia to be applied to eradicate Cr(VI) from the aqueous phase. The magnetic adsorbent exhibited an adsorption capacity of 154.0 mg/g [29]. Ma et al. [30] investigated the adsorption elimination of Cr(VI) from wastewater using the nanoscale zero-valent iron supported on PC-derived BC, which exhibited a removal performance of 39.05% at the typical experimental conditions. Saif et al. [31] reported the creation of AC from PC via carbonization of PC, followed by H_3PO_4

Figure 1. Images display pinecone.

Table 1. Precursors are used in the production of PO at multiple conditions

Precursor	Pyrolysis conditions	Yield (%) of product	Ref.
Orange peels	650 °C; 1 h; 10 °C/min	32.05% BC	[9]
Saga seeds	571 °C; 0.50 h; 271 cc/min N_2-flow	5.55% PO	[10]
Gold mohar	600 °C; 20 °C/min	48.0% PO	[11]
Manilkara zapota seeds	500 °C, 1 h; 80 °C/min, 1.0 mm particle size; 8:1 catalyst: feed; 100 cc/min N_2-flow	45.22% PO	[12]
Cashew skin	400 °C, 10 °C/min; 50 mL/min N_2-flow	37.10% PO	[13]
Mixed date stones and Pistachio shells	500 °C, 1.50 h; 20 °C/min, 50 mesh particle size	51.20% PO	[14]
African star apple defatted seeds cakes	400 °C, 1 h; 10 °C/min	33.10% PO	[15]
Chicken waste	500 °C, 2 h; 10 °C/min	61.60% PO	[16]
Beauty leaf fruit husk	500 °C; 3 min and 20 s	45.0% PO	[17]
Palm kernel cake	401 °C, 70 mL/min N_2-flow	63.0% PO	[7]
Ficus nitida wood	500 °C; 100°/min; 100 mL/min N_2-flow	41.85% PO	[18]
Date and cherry seeds	500 °C, 1 h; 40 °C/min, 0.25 mm particle size	55.55% PO	[19]
Date stones	500 °C; 10 °C/min, 1.50 mm particle size	36.64% PO; 16.12% BC	[6]
Flaxseed residue	500 °C, 60 mL/min N_2-flow	58.30% PO	[20]

activation of the resulting BC. The as-created AC was then implemented to reject various heavy metal ions, including Cr(VI), from wastewater with an adsorptive capability of 29.6 mg/g. Stripping Cr(VI) from the aqueous phase over the BC originating from PC was doped with zinc-doped nickel ferrite and then employed in extracting Cr(VI) from the aqueous solution with a removal efficiency of 95.0% [32]. Finally, the creation of AC from the pine needle employing the resultant AC to remove Cr(VI) ions from wastewater was announced by Ayoub et al. [33] who reported an adsorptive capacity of 65.36 mg/g.

Investigations relating to the creation of biofuel from PC are limited. Torrefaction of the North American PC was explored by McNamee et al. [34], who concluded that this process enhanced the fuel features of the PC, as well as raised its HHV and diminished its volatiles and moisture content. Kang et al. [35] used Ca–Fe and HZSM-5 to catalyze the thermal destruction of PC to create aromatic hydrocarbons and found that the said catalyst enhanced the deoxygenation and aromatization of the PC on pyrolysis in addition to lessening the emissions of PAHs. In another study, Chen et al. [36]

investigated pyrolysis-GC/MS experiments of the PC and the treated PC at 338 °C and 342 °C and found that the N content of the PC was above that of the treated PC. Also, with the increment of the conversion rate, the activation energies of the PC and the treated PC initially declined and then raised. Nonetheless, conducting thermal pyrolysis of PC with optimizing the experimental conditions that will lead to producing the maximum output of PO, including the temperature of pyrolysis, pyrolysis period, the particle size of PC, and the rate of heating, has not been announced yet as far as we know. Additionally, the complete analysis of the BO fraction separated from the resulting PO to recognize its chemical composition and its influential functional groups utilizing diverse techniques, like GC-MS, FTIR and ^{1}H NMR spectroscopy, in addition to its ultimate analysis has not been touched to the best of the author's knowledge. Moreover, exploiting the BC resulting from thermal pyrolysis of PC to create a high surface area microporous activated BC using the K_2CO_3 activation route with implementing the latter in the efficient elimination of Cr(VI) ions from wastewater has not been established yet.

2. Experimental

2.1. *Feedstock and chemicals*

The fresh precursor, PC, was brought from the forest area in Mosul city, north of Iraq. The PC was thoroughly washed with DW several times, followed by sun-drying for 48 h, crushing to a powder form, and finally sieving to acquire a particle size of 60 mesh. Iodine (I_2, solution, 0.1 N), $Na_2S_2O_3{\cdot}5H_2O$, 99.0–100.5%, K_2CO_3 (99.0%), and $K_2Cr_2O_7$ (99.90%) were of analytical reagent (AR) grade chemicals and were purchased from Scharlau chemicals, Spain.

2.2. *Proximate, ultimate, and thermogravimetric analyses of pinecone*

Based on the ASTM standard test methods, the PC weight percentages of moisture, volatile matter (VM), ash, and fixed carbon (FC) were quantified. The PC was placed in a silica crucible, heated to 110 °C in a hot air oven for 2 h, cooled to room temperature, and weighed. The dried sample left previously was implemented to quantify the VM% by heating a crucible containing it after being enclosed with a lid in a muffle furnace at 950 ± 20 °C for 7 min. The remaining solid was cooled inside a desiccator and weighed [37]. The weight loss represents the VM, while the solid residue is the FC. The residual carbon in the crucible was heated at 700 °C + 50 °C for 30 min without a lid. The crucible was preserved inside a desiccator to gain ambient temperature, and the solid residual solid was considered ash% [37]. The ultimate of the PC (C, H, N, and S) was carried out using an elemental analyzer (Elementar, Vario EL III, Germany). By difference, the O% was quantified. The analysis was accomplished on a dry basis. Based on the ultimate analysis results, the HHV of the PC was calculated as per Dulong's formula, presented in Equation (1) [38].

$$\text{HHV (MJ/kg)} = 0.3383 \times \text{C} + 1.443 \times \left(\text{H} - \frac{\text{O}}{8}\right). \quad (1)$$

Thermogravimetric analysis (TGA) of the PC was done employing a thermal analyzer (SDT-Q600 T.A. Simultaneous TGA/DSC, USA) to specify the thermal breakdown performance of the PC at a heating rate of 10 °C/min. The sample (~5 mg) was placed in a platinum crucible and heated between 35–1000 °C under a stream of N_2 gas and air. Finally, the PC contents of cellulose, hemicellulose, and lignin were identified utilizing the method proposed by Mansor et al. [39]. To specify the extractive % of PC, a known PC mass (5.000 g) was treated with 60 mL of acetone at 90 °C for 2 h, followed by drying at 105 °C and 100 °C. Weight difference before and after extraction represents the extractive %. After extraction, 1.000 g of the resulting material was treated with 150 mL of NaOH at 80 °C on a hot plate for 3.5 h to fix the hemicellulose %. After washing with deionized water, the sample was dried between 105 °C and 110 °C until attaining a fixed mass. The pre- and post-treatment weight differences signify the hemicellulose %. Determining the lignin % was accomplished by treating 1,000 g of the material remaining after the extraction with 30 mL of 98% H_2SO_4. After boiling the mixture at 100 °C for 1 h, the resulting mixture was filtered, while the solid residue was washed with 10% $BaCl_2$ solution before drying at between 105 °C and 110 °C. The mass alteration before and beyond extraction signifies the lignin %. The cellulose % was obtained by subtracting the PC's initial mass from the previously calculated weights of the other three constituents.

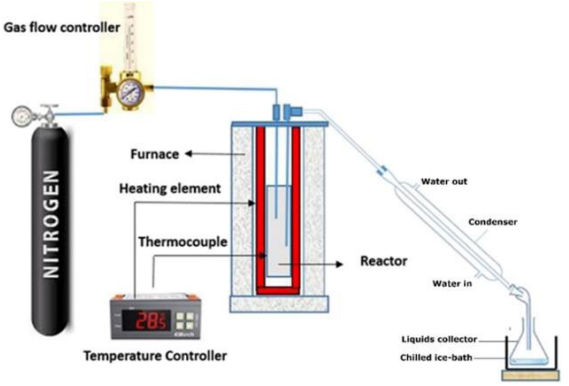

Figure 2. Pyrolysis reactor used in thermal cracking trails.

2.3. *Pyrolysis experiments of the pinecone*

The pyrolysis trails of PC were carried out in an inert atmosphere using a semi-batch reactor (Figure 2).

The pyrolysis reactor was cylindrical. It was built of stainless steel with a 30 cm length, 5 cm external inner diameter, and 4 cm internal diameter. The reactor was surrounded by an electrically heated cylindrical furnace and was provided with a PID controller to adjust the temperature and heating rate of the process. After feeding the reactor with the required PC mass (40 g), it was heated from ambient temperature until reaching the targeted temperature. The reactor was linked to a condenser to condense the volatile vapors, which were collected in a glass vessel placed in an ice bath (dry ice + acetone + salt). The reactor was blushed with N_2 gas (50 mL/min) for 15 min to expel the atmospheric oxygen before each experiment. Ultimately, the reactor was left to acquire ambient temperature, and the produced residue was collected as BC [40]. Calculating the yields of PO, BC, and non-condensable gases was completed based on the following equations [41,42]:

$$\text{Yield of Liquid (\%)} = \frac{\text{Weight of the PO produced (g)}}{\text{Total weight of PC used (g)}} \times 100 \quad (2)$$

$$\text{Yield of BC (\%)} = \frac{\text{Weight of BC (g)}}{\text{Total weight of PC used (g)}} \times 100 \quad (3)$$

$$\text{Yield of Gases and loss (\%)} = 100 - [\%\ \text{PO yield} + \%\ \text{BC yield}]. \quad (4)$$

The pyrolysis temperature (400–600 °C), the particle size of PC (0.26–0.841 mm), duration of pyrolysis (30–150 min), and the heating rate (10–50 °C/min) were optimized upon the thermal decomposition process of PC so as to disclose the typical settings that will produce the highest yield of the PO.

2.4. *Identification of pyrolytic oil*

The PO produced under typical thermal pyrolysis conditions of PC was fractionated into two fractions by a separating funnel. These fractions included the BO fraction (upper phase) and the aqueous fraction (lower phase). The BO fraction was identified for its functional groups using Fourier Transform Infrared spectroscopy (FTIR JASCO V-630, USA). The attenuated Total Reflectance (ATR) method was employed to analyze the BO. For this purpose, a small drop of the BO was placed on the ATR crystal, and the analysis was carried out in the range of 400–4000 cm^{-1} wave number at a 40 scanning with a step size of 4 cm^{-1}. The chemical composition of the BO was achieved using 1H NMR and GC-MS spectroscopy. The ^1H NMR spectra of BO were acquired on a Bruker 400 MHz NMR spectrometer (Bruker BioSpin, GmbH) with a 5.0 mm inverse triple resonance (TXI) probe for ^1H NMR. At the same time, $CDCl_3$ was employed as a solvent, and Tetra Methyl Silane (TMS) was implemented as the internal standard. The gas chromatography-mass spectrometry (GC–MS) spectrometry was employed to determine the composition of BO qualitatively and quantitatively. A GC–MS analyzer (Agilent 8860-5977B) under a stream of carrier gas (He) and a flow rate of 1 mL/min. The injector temperature and injection volume were respectively fixed at 280 °C and 1 μL. The oven program was originated at 60 °C (1 min), then elevated to 200 °C at 12 °C min^{-1} rate of heating, and lastly, the temperature was raised to 280 °C at a heating rate of 5 °C min^{-1}, where it was kept for 4 min [40].

2.5. *Biochar activation by K_2CO_3*

The BC produced upon the thermal degradation of the PC was utilized to prepare the AC. Firstly, the BC was ground by an electrical grinder, followed by sieving using a 60-mesh sieve. Synthesis of the ABC from the resulting BC was carried out through immersing a known mass of the BC (5.0 g) in solutions containing various impregnation ratios of the activator (K_2CO_3) on weight bases. The mixture was stirred for 5 h and left overnight in a desiccator. After drying at

105 °C for 5 h, thermal activation of the dried samples was accomplished in a muffle furnace at a given temperature and duration. The activated samples were then raised with a solution of 1.0 M HCl and washed several times until neutral water [43]. Synthesis of the ABC from BC was carried out by adjusting the activation conditions, including the ratio of the activator (0:5:1–3:1 w/w) and activation duration (30–120 min), as well as the activation temperature (550–850 °C). The yield of the AC was calculated based on Equation (1) [44]:

$$\text{AC yield (\%)} = \frac{\text{Maa of the produced ABC (g)}}{\text{Mass of BC used (g)}} \times 100. \quad (5)$$

2.6. *Characterization of the activated Biochar*

The surface physical morphology of the activated BC was perceived by the field emission scanning electronic microscope model (TESCAN MIRA FE-SEM, Czech Republic). The porosity and structural features of the AC carbon were examined by the N_2 adsorption–desorption isotherms model (A BELSORP MINI II, Japan, surface area and porosimetry analyzer). The BET method was applied to calculate the specific surface area of the AC. The GB/T 12496.8–2015 standard methodology was implemented to determine the iodine number (IN) of the so-produced AC [45]. An X-ray diffraction (XRD) model (a Malvern Panalytical X-ray diffractometer, UK) was employed to identify the crystal structure.

2.7. *Adsorptive elimination of Cr(VI) by activated biochar*

Following a batch method, the Cr(VI) adsorption tests were completed in 250 mL Erlenmeyer flasks. The batch adsorption studies evaluated the ABC performance under different pH, various Cr(VI) initial concentrations, the dosage of the ABC, the adsorption temperature, and the adsorption duration. To complete the adsorption trials, a mixture of the ABC and 50 mL of Cr(VI) solution were agitated at room temperature (25 °C) for a predetermined time until equilibrium was reached. The Cr(VI) solution was centrifuged at 5000 rpm for 15 min after adsorption. After separation, the Cr(VI) concentration in the clear supernatants was measured with an atomic absorption spectrometer (NOVA A350-analyitkjena-Germany). The adsorption removal percentage (AR%) of Cr(VI) was calculated as per Equation (2):

$$\text{AR (\%)} = \frac{(C_0 - C_e)}{C_0} \times 100, \quad (6)$$

where, C_0 and C_e signify the primary and equilibrium concentration (mg/L) of the Cr(VI), respectively. The amount of Cr(VI) adsorbed at equilibrium (q_e, mg/g) by the as-synthesized ABC was calculated using Equation (3):

$$q_e = \frac{(C_o - C_e)V}{W}, \quad (7)$$

where, V is the Cr(VI) solution volume (L), and "W" is the mass (g) of the ABC employed in the adsorption experiments, respectively.

3. Results and discussion

3.1. *Characterization of pinecone*

The possibility of implementing BM as a pyrolysis feedstock can be derived from its ultimate and proximate analyses. Table 2 shows the dry ultimate and proximate analyses of the PC compared with different lignocellulosic BM sources on a dry basis. From the ultimate analysis of PC, the latter had a higher C% than other lignocellulosic BM sources. Also, the PC exhibited an H% above that established for other lignocellulosic BM sources, but it was less than that reported for *Cascabela Thevetia* seeds [46]. The N% and S% in the PC were lesser than those established for other BO sources, and in some cases, the N% and S% of the PC were comparable. It was announced that the low N% and S% in a BM feed indicates that it will emit less SO_x and NO_x upon combustion [46]. Besides, the decreased S levels in a BM feed indicate less corrosion during the combustion or thermal pyrolysis [35]. Finally, the O% in the PC was, in most cases, below that established for other BM feeds. The low O% for BM feed will increase its calorific value besides producing BO with a low content of the O compounds [21,46].

In comparison with the ultimate analysis of PC samples in the literature, the C, H, N, S, and O contents of the PC used in the preparation of chemically AC were respectively 47.71%, 6.16%, 0.12%, 1.21%, and 44.80% [47]. On the other hand, the C, H, N, S, and O contents of the N-rich PC were respectively 43.99%, 3.65%, 1.67%, 0.51%, and 47.57% [48]. The

Table 2. The PC analysis results are compared with other BM feeds

Ultimate Analysis (on a dry bases)							
Biomass	C	H	N	S	O	H/C	O/C
PC	51.06	6.26	0.60	0.06	42.02	1.47	0.61
Acai seeds	43.29	5.98	1.29	0.10	47.59	1.65	0.82
Cascabela Thevetia seeds[b]	46.08	7.20	6.43	-	40.29	1.875	0.65

Biomass	Moisture %	Ash%	V.M.%	F.C.%	Calorific value (MJ/kg)
PC	4.55	0.92	75.30	23.78	18.72
Cascabela Thevetia seeds[b]	5.10	4.20	73.81	16.20	18.71
Castor seed hulls	4.40	6.71	72.05	16.89	13.85

Biomass	Extractive %	Cellulose %	Hemicellulose %	Lignin %
PC	7.0	33.50	36.60	22.90
Neem seeds[d]	29.24	38.04	21.94	13.58

[a]From Ref. [5]; [b]From Ref. [46]; [c]From Ref. [46]; [d]From Ref. [46].

elemental analysis outcomes of the PC used in this study were comparable to some of those mentioned above. Nonetheless, variations in the elemental composition of varied PC samples worldwide could be ascribed to the type of soil where the PC trees are planted, besides the soil's chemical composition and the country's climate.

The proximate analysis outcome of the PC disclosed that its contents of moisture, ash, volatile matter, and fixed carbon were 4.55%, 0.92%, 75.30%, and 23.78%, respectively. For the moisture % of the PC, it was below that reported for *Cascabela Thevetia* seeds [46] and coaster seed [46] but comparable to that of the castor seed hull [49]. Ahmad et al. [50] declared that a 10.0% moisture content in the BM feed is recommended as a pyrolysis precursor. The volatile material % for the PC was above that reported for the other BD feeds tabulated in Table 2. According to Ahmad et al. [50], the production of gases and liquid products increases when the BM feed possesses a high volatile matter %. Also, the produced fuel will have a higher ignition performance. The PC had a fixed carbon % above that announced for *Cascabela Thevetia* seeds [46] and castor seed hull [49], but it was comparable to that established for other BM feeds presented in Table 2. The fixed carbon % for the PC suggests its suitability for being utilized successfully in pyrolysis [51]. The ash% of the PC was comparable to that of the castor seed hull [49], but it was below that established for other BM feeds presented in Table 2. This parameter must be as low as possible, as it adds several adverse effects on the feature of the BM feed, like the low heating value, formation of slag, and corrosion or blockage of the equipment [46]. As per the literature, the FC%, VM%, and ash% for a sample of PC in the literature were respectively 23.41%, 73.98%, and 2.61% [47]. These findings are comparable to those established for the PC sample used in this work. However, the variations in the FC%, VM%, and ash% for varied PC samples worldwide may belong to the chemical composition of the PC samples besides the standard procedures followed upon determining these features.

The extractive % for the PC was below that announced for other BM seeds. This outcome is expected as these seeds contain a high percentage of oil, which raises its extractive %. The content of lignin for the PC was above that of neem seeds [46] and below that of coaster seeds [46]. Higher lignin content in the BM feed favors char formation during pyrolysis [34]. Finally, the calorific value of the PC was comparable to that of *Cascabela Thevetia* seeds [46] but higher than that reported for the castor seed hull and coaster seed. As per the properties of the PC, it can be utilized as a thermal pyrolysis precursor. Moreover, the component analysis of any BM feed has a potential impact on its thermal pyrolysis behavior as an outcome of the percentages of the components in the parent feed, which in turn affects the output of its pyrolysis products.

The thermal degradation behavior of any BM feed can be estimated by thermogravimetric analysis (TGA). The TGA examination of the PC accomplished at a 10 °C/min heating rate in a temperature range of 35 to 1000 °C under a stream of N_2 gas and air is presented in Figure 3, which confirmed that, like any BM feed, the thermal decomposition of PC possessed through three chief periods, namely drying, devolatilization, and char creation zone [52]. The drying zone (1st stage) started from ambient to 150 °C. This stage mainly excludes unbonded water molecules and some very lightweight ingredients [53]. The devolatilization period (2nd stage) is also named the active pyrolysis step. This stage initiated from 150 °C to 550 °C. This stage involves the thermal degradation of the heavier molecule as an outcome of the larger heat supply. During this period, the greatest quantities of hot volatiles are generated as a consequence of the thermal decomposition of the PC components, viz. hemicellulose, cellulose, and a slight lignin [54]. The last zone of thermal destruction is the 3rd stage, also called the char formation zone. This stage usually occurs at a temperature above 550 °C and is primarily ascribed to the thermal degradation of lignin at a prolonged rate [55]. The DTG thermograph (Figure 3) disclosed that nearly 10% of the PC was decomposed in the 1st pyrolysis stage, while about 70% of the decomposition occurred in the 2nd. Moreover, the first peak in the DTG thermogram belongs to the moisture and mild volatile component elimination at a temperature above 150 °C. Based on the literature, cellulose and lignin degrade at temperatures above that of hemicellulose [56,57]. Hemicellulose and cellulose decomposition peaks occurred at temperatures between 200–500 °C. Lignin degradation starts at 180 °C, but its degradation is prolonged and continues at higher temperatures (>500 °C). Char generation upon pyrolysis is influenced by lignin composition. A higher lignin content in BM leads to increased char production. Additionally, higher energy is needed to trigger the reaction [58]. Comparable performance was also observed in the present study, with minor differences due to differences in the composition of the raw BM feed [58]. Notably, the thermal decomposition behavior of the PC used in this work was analogous to that established for other PCs in the literature [58,59]. These studies disclosed that the active devolatilization zone of the PC samples was nearly between 200 °C and 500 °C. Nonetheless, the minor differences in the percentages of the decomposition stages may be ascribed to the type of inert gas used upon performing the TGA measurement besides the heating rate of the decomposition process.

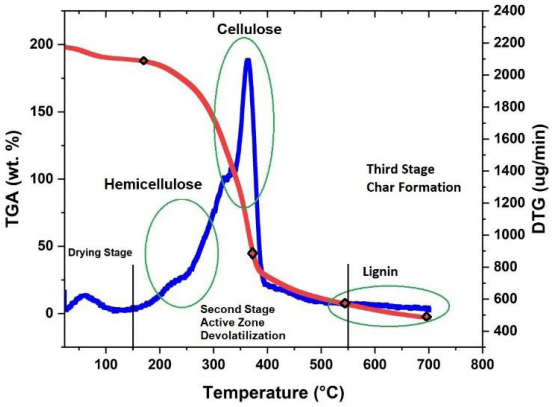

Figure 3. TGA-DTG thermograms of the PC.

3.2. *Optimization of thermal pyrolysis parameters*

Thermal pyrolysis of the PC in a fixed-bed reactor was accomplished to analyze the influence of the process parameters, including pyrolysis temperature, pyrolysis time, particle size of the PC, and heating rate on the PO, BC, and gas yields, as presented in Figure 4(a–d). However, during the optimization of the thermal pyrolysis experiments, the PO output was adopted as a starting point to transfer from one variable to the following variable until reaching the typical pyrolysis variables that will lead to producing the maximum output of the PO.

It is clear from Figure 4(a), which examines the influence of the pyrolysis temperature of the PC on its product yields. The PO yield was low at 400 °C because of the incomplete pyrolysis of the PC. Low pyrolysis temperatures are associated with limited heat and mass transfer of the BM particle inside the reactor, causing a low PO output. When the temperature increased above 400 °C, the PO yield reached a maximum of 500 °C. At this temperature, the heat and mass transfer between the PC particles will be maximum because of the longer contact time, which permits the complete transformation of the PC into volatile products [14,42]. So, the yield of the PO is

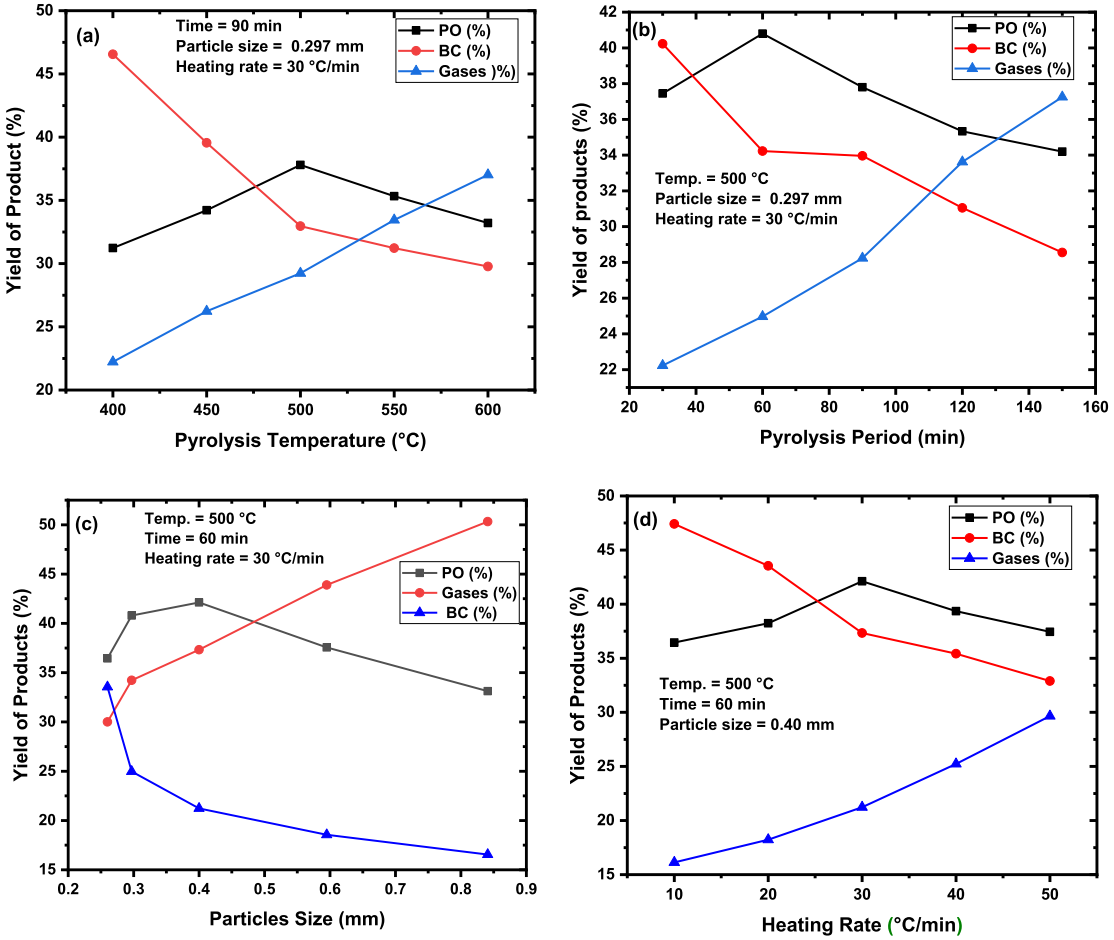

Figure 4. The pyrolysis parameters influence on the product yields.

enhanced. Beyond 500 °C, the output of the PO reduced may be due to the transformation of the PC at higher temperatures into non-condensable vapors as a consequence of the secondary thermal destruction reactions, which enhance the PC fragmentation besides the produced PO into non-condensable products (CO, CO_2, CH_4, H_2, etc.) [14]. On the other hand, the output of the BC diminished with increasing thermal pyrolysis temperature while the gas yield rose. These consequences originated from the secondary thermal destruction reactions of the feed and BC as an outcome of the quick endothermic degradation of the produced BC into non-condensable gases. The production of the highest yield of the PO from the PC at 500 °C was comparable to the typical temperature for thermal degradation of various BM sources, like mixed date stones, pistachio shells stones [14] and babool seeds [60]. However, a maximum pyrolysis temperature of 500 °C was less than that required for thermal destruction of Mahua seed (525 °C) [61].

The period at which the precursor spends inside the pyrolysis reactor is one of the variables determining the pyrolysis product output. It was reported that the pyrolysis completion is highly connected to the pyrolysis period since shorter intervals may lead to partial feed degradation. Furthermore, to undergo thermal cracking, the feed must remain in the reactor for an extended period upon the cracking so as to allow heat to spread throughout the entire particle [61,62]. Therefore, it is essential to determine the ideal time for the pyrolysis process. The thermal degradation of the PC was tested over several intervals (30–150 min) while retaining other variables,

as presented in Figure 4(b), which showed that the higher liquid output was obtained by lengthening the pyrolysis period from 30 min to 60 min, the PO output boosted from 37.45% to 40.80%. Such an outcome suggests that a period of 60 min is sufficient to condense all the volatile vapors produced upon thermal degradation of the parent feed. Nonetheless, beyond this duration, the PO output declined due to the continuous thermal degradation of the authentic feed besides the produced volatiles into non-condensable vapors [10]. On the other side, an increase in the gaseous yield and a diminish in the BC yield were noticed when the duration of pyrolysis increased as a consequence of the additional gasification of the parent feed, PO, and the produced BC into non-condensable vapors at the expense of the BC yield [10,12,16]. The thermal pyrolysis of mixed date and cherry seeds [19] and pistachio shells [62] resulted in similar findings.

The mass and heat transfer within the pyrolysis zone is greatly affected by the feed's particle size, thus affecting the output of the pyrolysis product. It was reported that large particles prefer char formation upon thermal pyrolysis while producing gases and liquid products prefer smaller particles [40]. Accordingly, thermal destruction of the PC was carried out employing particles of various sizes (0.25, 0.297,0.4, 0.595, and 0.841mm), with maintaining temperature, time, and rate of heating fixed at 500 °C, 60 min, and 30 °C/min, respectively. It was found that with decreasing the particle size, the PO yield rose as a consequence of increased heat and mass transfer, which offered an entire conversion of BM feed into products [19]. The highest yield of the PO was produced employing particles of 0.40 mm size. Figure 4(c) exhibited that particles of the bigger size prefer the production of BC rather than other products because of the incomplete transformation of the BM feed. Thus, the heat transfers between the BM feed particles fall, causing a decline in the yields of the PO and gases. Mishra and Mohanty announced similar observations on the thermal degradation of *Samanea saman* seeds [41].

Among the experimental variables that have an essential impact on the product's yield upon the thermal destruction process is the rate of heating of the feed inside the reactor. Thus, it is necessary to find out the typical heating rate of the BM feed during the thermal cracking process. To do so, thermal pyrolysis of the PC was accomplished at multiple heating rates ranging from 10 °C/min to 50 °C/min, preserving other factors at their optimal values. Based on the findings in Figure 4(d), the lowest output of PO and gases and the highest production of BC were obtained at the lowest heating rate. Such findings could be ascribed to the imperfect thermal destruction of the authentic PC particles inside the reactor as an outcome of the insufficient mass and heat transmission among the PC particles [40,42]. An improvement in the PO yield from 36.45% to 42.12% was noticed as the rate of heating rose from 10 °C/min to 30 °C/min, as a possible increase in the mass heat and conduction among PC particles. As an outcome of the endothermic cracking of the PC (rapid fragmentation reactions), heating rates beyond 30 °C/min caused a diminish in the PO yield [19]. Figure 4(d) also clarifies that the BC yield decreased, while increased gaseous product yield was noticed with increasing heating rate. This outcome suggests the PC's quick decomposition into non-condensable gases due to the secondary thermal destruction reactions [18,19]. Al-Layla et al. [40] and Mishra et al. [41] reported similar consequences upon the thermal decomposition of milk thistle and *Samanea saman* seeds, respectively. As we stated earlier, determining the typical experimental conditions of the thermal pyrolysis of PC was based on the conditions that will lead to produce the highest output of the PO. So, as per outcomes presented in Figure 4, the highest yield of the PO (42.12%) was produced using 0.40 mm particle size of the PC at 500 °C for 60 min and 30 °C/min rate of heating.

3.3. *Identification of PC-derived bio-oil*

The PO produced at the typical experimental conditions (500 °C, 60 min, 0.40 mm particle size, and 30 °C/min heating rate) was fractionated in a separating funnel into the BO and aqueous phases. The BO yield amounted to 10.20% of the total weight of the PO. This BO was identified for its chemical composition and ultimate analysis.

3.3.1. ^{1}*HNMR analysis*

Table 3 demonstrates the % of different kinds of H defined by the chemical shift results of the BO created through pyrolysis of PC. At the same time, Figure 1S (supplementary material) shows the ^{1}H NMR

spectra of BO. The ^{1}H NMR spectrum for the BO obtained by thermal destruction of PC at 500 °C showed that the region between 6.50 ppm and 7.0 ppm suggested that the as-created BO contains multiple functional groups. The ^{1}H NMR spectra of the as-created BO revealed three key areas: aliphatic, olefinic, and aromatic [40,61–63]. Nonetheless, the area between 0.50–3.0 exhibited crowded peaks belonging to the aliphatic fraction of the BO, whereas peaks in the region between 4.5–6.3 ppm express the olefinic part. Chemical shifts between 6.0 and 9.0 ppm best characterize the aromatic resonances [40,61]. Based on the above findings, the as-synthesized BO was predominantly composed of aliphatic structural components. Aliphatic hydrocarbons comprised 89.34% of the BO, while aromatic hydrocarbons constituted 7.0%. The ^{1}HNMR measurements of the acquired BO are consistent with those obtained from other BO samples synthesized from various precursors, like the dried black liquor solids [64], tobacco processing wastes [65], and algal waste [66]. The BO samples originating from these precursors disclosed that the major peaks were crowded in the region belonging to the aliphatic fraction of the BO. So, following the ^{1}H NMR outcomes, it can be concluded that the resulting BO consisted of many H atoms originating from the aliphatic CH_3–, CH_2– and CH– groups [66]. Nevertheless, the difference in the types of H that occurred among the BO samples in the literature could be ascribed to many issues, including the chemical composition of the parent BM feed, the pyrolysis circumstances, and the kind of feedstock employed.

3.3.2. *Ultimate analysis of bio-oil*

Table 4 compares the contents of C, H, N, S, and O of the BO separated from the resulting PO under the optimal experimental conditions with other BO samples produced from various feedstocks in the literature. Following the outcomes presented in Table 4, the C% of the BO derived from thermal pyrolysis of PC was above the contents of other elements, and such an outcome is expected, as C is the main element in any BM feed. It was also noticed that the C% of the BO originated from thermal pyrolysis of PC, which was above that established for BO samples created from various BM feeds in the literature. It was reported that the high C% of BO raises its heating value [40]. Besides, the H% of the produced BO was greater than that established for other BO samples in the literature (Table 4). The H/C molar ratio of the as-produced BO was 1.27, implying that it ranges between light and heavy petroleum oils [19]. Furthermore, the H/C molar ratio of the BO produced from the thermal degradation of PC was above that declared for BO samples originating from the pyrolysis of *Samanea saman* seeds [41], cotton seed [15], and Tung seed residues [64]. It was established that the amount of heat produced upon the combustion of BO is highly related to its H/C [67]. Sultana et al. [68] announced that the H/C molar ratio affects the aromatization degree of BO, in addition to other factors, including the presence of a catalyst, the chemical composition of the BM feed, and conditions applied to the pyrolysis process. On the other hand, it was noticed that the BO produced from the PC had a lower O% than the pristine PC as an outcome of the transformation of the oxygenated hydrocarbons in the parent feed into non-condensable gases [35]. Besides, the O% in the as-created BO was below that established from mixed date stones and pistachio shells [14], Samanea saman seeds [41], and Tung seed residues [67]. It was established that the BO with a lower O% will be less corrosive and needs lower upgrading conditions besides having a higher calorific value [41]. It is evident from Table 4 that the N% and S% of the produced BO were below those announced for BO samples from other BM feeds (Table 4). Such lower values of O% and S% suggest that the BO emissions of NO_x and SO_x will be less [14,41]. The calorific value (HHV) of the BO resulting from thermal pyrolysis of the PC was above that announced for BO samples originating by thermal destruction of various BM feeds (Table 4). Such an outcome could be ascribed to many factors, such as the H/C molar ratio of the parent feed besides the chemical composition (its contents of cellulose, hemi cellulose, and lignin).

3.3.3. *GC-MS analysis of bio-oil*

The GC-MS analysis can better recognize the variety of components found in BO. Because of its complex composition, it was declared that BO comprises more than 300 chemical components [41]. Aliphatic, oxygenates, nitrogenates, heterocyclic, monoaromatics, and polyaromatics were the six primary categories into which these compounds were sorted [40]. According to the literature, most BO samples contain esters, ethers, amines, nitriles, aldehydes, ketones,

Table 3. Hydrogen types deduced from ^{1}H NMR spectroscopy

Type of H	Chemical shift (ppm)	H%[a]	H%[b]	H%[c]	H%[d]
Aromatic, CHO	6.0–9.50	9.69	7.53	13.09	25.45
Phenolic (O–H) or olefinic proton	4.50–6.0	-	19.86	-	6.64
CH_3–C=O, CH_3–N, –CH_3–C	3.0–4.50	18.27	7.21	1.34	5.99
Aliphatic and α-hetero atoms	1.5–3.0	38.07	19.86	54.42	29.61
CH_3, CH_2 and alkanes	0.0–1.50	45.36	7.53	31.15	32.31

[a]BO from PC; [b]BO from dried black liquor solids [64]; [c]BO from tobacco processing wastes [65]; [d]BO from algal waste [66].

Table 4. Ultimate analysis of the PC-derived BO (dry bases)

BO source	C%	H%	N%	S%	O% by difference	H/C	O/C	Calorific value (MJ/kg)	Ref.
PC	65.04	6.87	0.36	0.02	27.71	1.27	0.31	26.99	This work
Mixed date stones and pistachio shells	60.50	6.84	0.30	-	32.06	1.35	0.39	24.54	[14]
Cotton seed	62.66	2.06	3.45	-	31.83	0.39	0.38	23.14	[15]
Samanea saman seed	61.47	4.01	3.47	1.88	29.17	0.78	0.17	21.23	[41]
Tung seed residues	60.63	4.56	0.43	0.06	34.52	0.91	0.43	22.89	[67]

and acids [40,41]. Following the findings presented in Figure 5, the BO synthesized from the thermal decomposition of PC contained different organic compounds, and the O-organic compounds prevailed. These compounds were composed of phenols (63.55%), alcohols (16.57%), ketones (6.85%), furans (5.45%), aromatics (2.92%), acids (1.16%), and hydrocarbons (1.30%). The resulting BO contained a minor ratio of nitrogenate (0.33%). Acetic acid and furans are the most common byproducts of woody BM pyrolysis [7]. The degradation of lignin in PC also yields other phenolic compounds, including phenol, methyl phenol, methoxy phenol, methyl methoxy phenol, ethyl methoxy phenol, vinyl methoxy phenol, eugenol, and propenyl methoxy phenol [69]. The GC-MS spectrum is presented in Figure 2S (supplementary material), while Table 1S lists all chemical compounds present in the as-produced BO detected by the GC-MS.

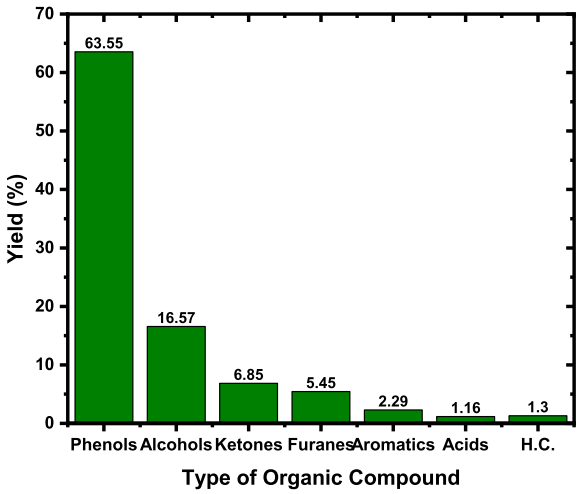

Figure 5. Types of organic compounds present in the BO.

3.4. *Optimization of activated biochar synthesis*

The K_2CO_3 activation method was employed in converting the BC leftover from the thermal decomposition of the PC. One of the most effective factors affecting both the yield and surface area of the ABC production is the molar ratio of the activator. The activator is the key factor responsible forming the porous structure of the ABC as an outcome of the

chemical reactions occurred as the precursor and the activator mixture is subjected to heat upon activation, including dehydration reactions. So, finding the proper molar ration of the activator must be specified. The effect of activator impregnation ratio (IR), temperature, and duration on ABC yield and IN were explored to reach the typical conditions that will lead to the development of the best ABC sample. It was shown that the ABC production dropped as the activator's IR increased. This result suggests that tar and other volatile compounds are released from the BC at higher activator concentrations, leading to a drop in the ABC yield [19,44]. Furthermore, as an additional activator is added, more C atoms in the feed skeleton will break down due to their reaction with the activator, besides further burning off the sample, thus lowering the ABC output [44]. Similar findings were established upon K_2CO_3-activation of the BC resulting from co-pyrolysis of mixed date and cheery seeds [19]. As the activator quantity rose from 1:1 to 2:1, as shown in Figure 3S(a), the microporosity of the ABC pointed out by the IN improved, indicating that the latter IR is typical to construct a more microporous structure ABC. When BC was overactivated with excessive activator concentrations (>2:1), the walls of the adjunct micropores broke down and bigger pores (meso- or macro-pores), and thus the IN turned down [70].

The temperature of activation offers an immense effect on the yield and porosity of ABC. As indicated in Figure 3S(b), higher activation temperatures decreased the ABC yield as a consequence of the thermal pyrolysis of lignin with the increment of temperature above 600 °C. Also, chemical activation by K_2CO_3 initiates between 450 °C and 500 °C and involves two phenomena, pyrolysis and activation of lignin with K_2CO_3, leading to the gasification of carbon in the structure of the feed into CO besides the degradation of K_2CO_3 into K_2O, as follows [70]:

$$K_2CO_3 + 2C \rightarrow 2K + 3CO \quad (8)$$

The K_2CO_3 may also suffer from thermal decomposition into CO_2 and K_2O, and the occurrence could cause further activation of the feed, as follows:

$$C + CO_2 \rightarrow 2CO \quad (9)$$

$$2K_2O + C \rightarrow 4K + CO_2 \quad (10)$$

Such a reaction will cause a diminish in the ABC output. Figure 3S(b) shows that raising the activation temperature from 550 to 750 °C produced more micropores in the ABC structure. This occurs as an outcome of the above chemical reactions, which result in the gasification of the authentic feed into CO and CO_2, leaving behind an ABC with a well-developed microporous structure and thereby improving the IN [19,44,70]. The degradation of the ABC microporous structure caused a drop in the IN at temperatures beyond 750 °C [19,71], which may be due to harsh degradation of the feed besides the produced ABC structure into non-condensable gases, which in turn causes a widening in the microporous [19].

The activation time during the synthesis of ABC needs to be optimized due to its economic significance. Figure 3S(c) revealed that an increase in duration resulted in a decline in the ABC yield, which was caused by the aggressive burn-off of the parent BC as a consequence of the prolonged activation period at high temperatures [44]. The IN increased when the activation time was raised from 30 to 60 min, according to Figure 3S(c). This outcome suggests that by extending the activation time at an elevated temperature, the pore created as a result of the activation will be blocked by the evolved volatile matter. So, with extending time, these vapors will be expelled out of the resulting porous structure of the produced ABC. Nonetheless, activation periods beyond 60 min diminished the IN of the resulting ABC, as an outcome of the microporous blockage by vapor evolved upon thermal activation, resulting in a diminish in the IN [44,71].

3.4.1. *Identification of K_2CO_3-activated biochar*

After synthesizing the best ABC sample at the optimal activation settings (2:1 K_2CO_3: BC, 750 °C; 1 h), surface texture, morphology, and the crystalline structure were identified using the N_2-adosotion–desoprtion isotherms at 77 K, FESEM, and XRD, as demonstrated in Figure 6. The FE-SEM specified the morphology assessment of the ABC surface. Figure 6(a) shows that the ABC had a rough, uneven surface with some granules. Furthermore, fissures, holes, and cavities of different sizes were also noticed on the ABC surface. Such cracks and cavities, alongside the pores, will allow the adsorption of various molecules to enter them more quickly, leading to a high elimination efficacy. Figure 6(b) shows the XRD pattern of the ABC, as previously mentioned. It showed the presence of two immense specific peaks

associated with the (002) and (101) phases of amorphous carbon, located at 2θ = 24° and 2θ = 44° [72]. In addition to the pore size distribution curves of the ABC, as constructed, Figure 6(c) shows the N_2 adsorption–desorption isotherms. At low relative pressure ($P/P_0 < 0.05$), the ABC N_2 uptake curve abruptly increased before plateauing, indicating that the isotherm represented type I, a characteristic of microporous materials [72]. The ABC created above showed a SA_{BET} of 465.55 m^2/g and a mean pore diameter of 1.97 nm, affirming its microporous structure. The surface area of the ABC developed by the direct chemical activation of PC by KOH amounted to 478.89 m^2/g [73]. In comparison, the direct activation of the PC by H_3PO_4 produced an ABC having a BET surface area of 1597 m^2/g [74], compared to 1823 m^2/g for that developed by the direct activation of PC by $ZnCl_2$ [74]. Nonetheless, besides the synthesis conditions, the type of activator used in preparing ABC potentially impacts the texture of the resulting ABC.

3.4.2. *Application of ABC in Cr(VI) removal*

The ABC prepared under the typical experimental conditions was tried to eliminate Cr(VI) ions from its aqueous phase. The investigation was performed by optimizing the experimental conditions affecting the process. One of the variables that possesses an energetic influence on the adsorption of Cr(VI) from solution is the initial pH of the solution, as this parameter affects the electrostatic combination of the Cr(VI) species with the surface of the ABC [75]. So, assessing the pH effect on the AR of Cr(VI) from solution by the as-developed ABC was accomplished by conducting the adsorption of Cr(VI) from a solution having different pH (2, 4, 6, 7, and 8) while keeping other variables fixed as given in Figure 7(a). This figure disclosed that increasing the solution's pH from 2.0 to 8.0 caused a decline in the AR% of Cr(VI) from the aqueous phase. The highest AR% was obtained at a pH = 2.0, while beyond this value, the AR% declined progressively, which is consistent with former studies [76,77]. In the acidic environment (pH < 6.0), the surface of the resulting ABC can be positively charged through the interaction with the extra H+, which in turn augments the adsorption of negatively charged anions of Cr(VI). As the solution's pH rises, competition between the OH– and anionic groups containing Cr(VI) for the active sites will occur, preventing Cr(VI) removal [75–77].

The effect of various Cr(VI) ion concentrations in the range of 25–150 mg/L on the AC adsorption performance was evaluated. The setup in which the trials were conducted is indicated in the legend of Figure 7(b). As the concentration of Cr(VI) ions rose from 25 ppm to 150 ppm, the amount of Cr(VI) ions absorbed by the ABC rose from 9.87 mg/g to 57.96 mg/g. This effect results from the high concentration ascent, which will motivate the species of Cr(VI) ions to proceed toward the ABC active locations, resulting in better pollutant adsorption [75]. Similar findings were declared upon the AR of Cr(VI) from wastewater over some biowaste-derived adsorbents [78,79].

To analyze the impact of the ABC dose on the AR% of Cr(VI) ions, a series of experiments were conducted using varying amounts of the ABC, ranging from 0.10 g to 0.40 g. Concurrently, other conditions were established, as illustrated in Figure 7(c). Trying more ABC amounts enhances the AR% of Cr(VI) ions. This is because as the ABC mass employed in the adsorption process increases, the number of particles (or active binding sites) responsible for the AR of the pollutant [77,78]. When 0.20 g of the ABC was tried, the maximum AR% efficiency was reached. Amounts beyond 0.20 go of the ABC lessened the AR% of Cr(VI) ions. This finding could be because the additional doses of ABC may congregate and overlap ABC particles, reducing the number of active sites available to remove the pollutant and causing a decline in its AR% [74].

The effect of the adsorption temperature on the AR% of Cr(VI) ions by the as-created ABC was investigated from 15 °C to 55 °C while maintaining other circumstances constant, as presented in the legend of Figure 7(d). The AR% of Cr(VI) ions enhanced as the temperature rose from 15 °C to 35 °C, then decreased. At 35 °C, the highest AR% of Cr(VI) ions was achieved. The solution's viscosity declines as temperature rises, allowing Cr(VI) ions to diffuse into ABC pores and improve the AR% [73,85]. Moreover, collisions between the ABC particles with ions of Cr(VI) enhance as the adsorption temperature rises, causing higher elimination of the Cr(VI) ions from the solution [85]. The decrease in AR% of Cr(VI) ions beyond 35 °C may be due to the desorption of the pollutant ions from the ABC surface into the solution [73].

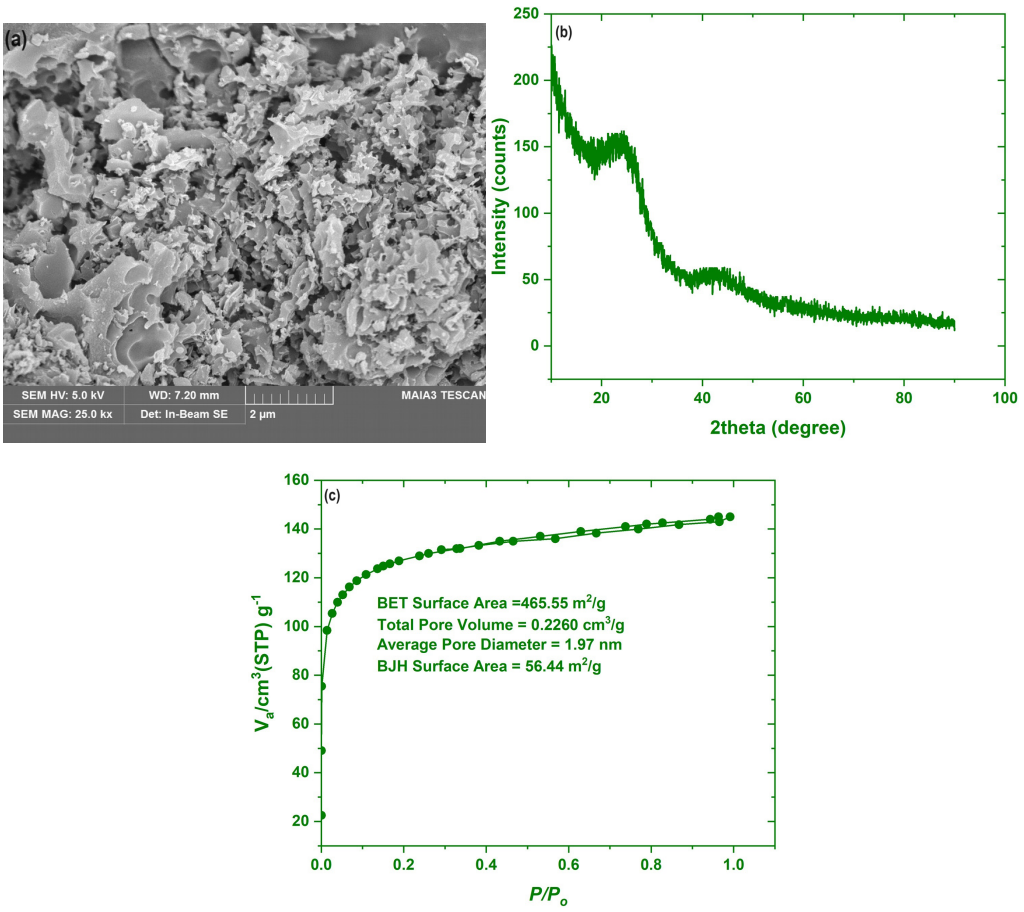

Figure 6. The FESEM image, XRD patterns, and N_2 adsorption–desorption isotherms of the ABC.

Table 5. Adsorption isotherms values and Q_m value for the ABC and other adsorbents

Type of isotherm					
Langmuir isotherm			Freundlich isotherm		
R^2	Q_m (mg/g)	K_L (L/mg)	R^2	K_F (mg/g)/(mg/L)$^{1/n}$	n
0.9911	62.90	0.4300	0.9811	20.45	1.69

Comparison of Q_m for Cr(VI) adsorption by the ABC compared to other adsorbents			
Adsorbent	Q_m (mg/g)	Isotherm	Ref.
Magnetic AC	57.80	Langmuir	[80]
Fe_3O_4 NPs	25.06	Langmuir	[81]
Peach stones-derived AC	14.05	Langmuir	[82]
Mango kernel-derived AC	7.10	Langmuir	[83]
Nutshell-derived AC	46.20	Langmuir	[84]
ABC	62.90	Langmuir	This work

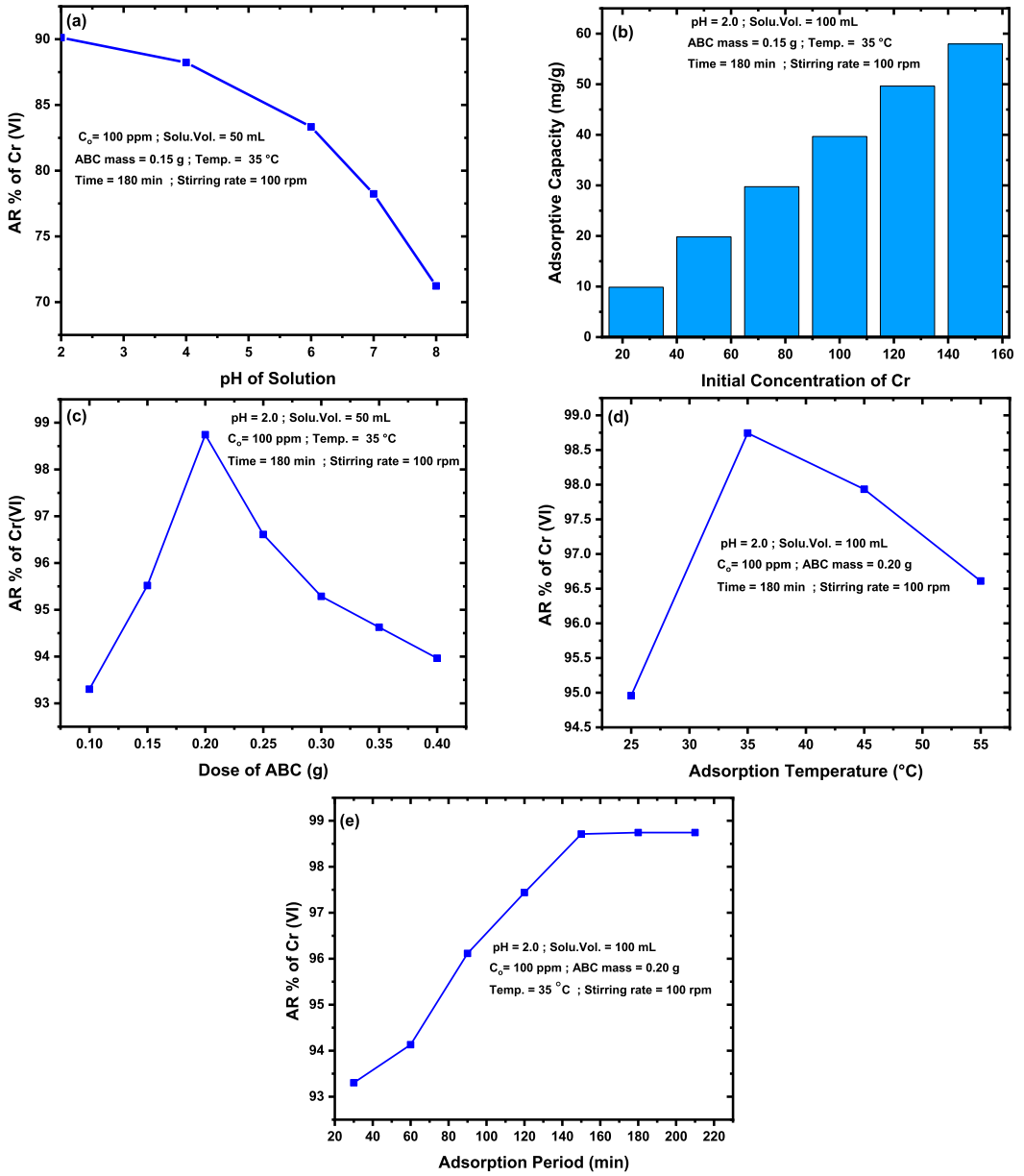

Figure 7. Effect of adsorption variables on the Cr(VI) adsorption by the PC-derived ABC.

It is necessary to examine the point at which a system reaches equilibrium from an economic perspective. Thus, varied durations (30–120 min) were examined upon exploring the effect of time on the AR% of Cr(VI) ions from its solution while preserving other parameters at their ideal values. The information provided in Figure 7(e) showed that the adsorption duration had a desirable effect on the AR% of Cr ions by the ABC. The equilibrium was attained at 150 min, while the prolonged period had no further impact on the ABC because empty holes existing for the adsorption no longer occur [73,85].

3.4.3. *Adsorption isotherms of Cr(VI) by the activated biochar*

The adsorption isotherms of Cr(VI) adsorption over the as-produced ABC were analyzed using the Langmuir and Freundlich isotherms, and their non-linear equations and plots are offered in Table 1S and Figure 4S (supplementary material).

It was reported that the Langmuir isotherm proposes that the adsorption of an adsorbate on a given adsorbent is homogenous and mono-layer [86]. On the contrary, Freundlich suggests that the adsorption is heterogeneous and multi-layers [85]. After analyzing the adsorption outcomes of Cr(VI) by the as-synthesized ABC, it was concluded that the adsorption of Cr(BI) by the ABC is possible, as the value of R_L (separation factor) was above 0.0 and less than 1.0. Also, the value of n was above 1.0 [86,87]. However, the Langmuir model best described the adsorption of Cr(VI) by the ABC, as this model exhibited a higher correlation coefficient (R^2) compared to the Freundlich isotherm, demonstrating that the adsorption of the said pollutant by the ABC was homogenous and mono-layer. Table 5 displays values of the constants relating to the adsorption isotherms. It also compares the maximum adsorption capacity (Q_m, mg/g) of Cr(VI) adsorption over the as-produced ABC to other adsorbents in the literature. It was noticed that the Q_m value for Cr(VI) adsorption by the as-produced ABC was above that established for other adsorbents. Nonetheless, the variance in the Q_m values for different adsorbents could be ascribed to many factors, including the surface area and mean pore diameter of the adsorbent, the initial concentration of the pollutant in the examined solution, and amount of the adsorbent used in the AR process. Accordingly, the ABC developed from the PC has the potential to be applied on the industrial scale.

3.4.4. *Adsorption mechanism*

The solute's adsorption mechanism must be explored on the adsorbent solid surface to remove various pollutants from an aqueous phase. Mechanism of the pollutant's adsorption from the liquid phase involves several mechanisms, such as ion exchange, dipole–dipole, chemical bonding, dipole–induced dipole, and H-bonding [88–90]. However, the pore-filling mechanism, which significantly depends on the adsorbent surface area, remains the primary mechanism for eliminating pollutants from the liquid phase, while another mechanism could be axillary. So, the above mechanisms could eliminate Cr(VI) from the liquid phase [73,90].

4. Conclusions

Thermal pyrolysis of PC in a fixed-bed reactor showed that the operation conditions affected the maximum yield of the PO. The highest yield of the PO amounted to 42.12% at 500 °C for 1 h using 0.40 mm particle size with a 30 °C/min rate of heating. Moreover, the BO content in the produced PO was 10.20%. The BO was mainly composed of oxygenated compounds, which amounted to 54.98%, besides the N-organic compounds and hydrocarbons, whose contents were 6.95% and 2.60%, respectively. Besides, the BO exhibited a high content of C and H besides its high caloric value (26.99 MJ/kg). Activating the BC leftover from the pyrolysis of PC with K_2CO_3 produced a microporous ABC with 465.55 m^2/g and 1.97 nm average pore diameter using 2:1 K_2CO_3: char at 750 °C for 1 h. This ABC was also implemented in the adsorptive elimination efficiency of 150 mg/L Cr(VI) solution, which amounted to 98.71% utilizing 0.20 g of the ABC at 35 °C for 150 min and a pH of 2.0. Besides, the adsorption of Cr(VI) by the as-produced ABC followed the Langmuir adsorption isotherm. In conclusion, PC could be used as a pyrolysis feedstock for producing high-content aromatic oxygenates BO, as well as ABC, with a high surface area and a well-developed microporous structure.

List of abbreviations

BM	Biomass
PC	Pinecone
PO	Pyrolytic oil
BC	Bio-char
BO	Bio-oil
HHV	Higher heating value
AC	Activated carbon
ABC	Activated bio-char
TGA	Thermogravimetric analysis
GCMS	Gas chromatography-mass spectroscopy
^{1}H NMR	Proton magnetic nuclear spectroscopy
BET	Brunauer–Emmett–Teller
FESEM	Field emission scanning electron microscope
XRD	X-ray diffraction
AR	Adsorptive removal

Declaration of interests

The authors do not work for, advise, own shares in, or receive funds from any organization that could benefit from this article, and have declared no affiliations other than their research organizations.

Acknowledgements

We thank Mosul University, College of Science, Department of Chemistry for supporting this research work.

Supplementary data

Supporting information for this article is available on the journal's website under https://doi.org/10.5802/crchim.351 or from the author.

References

[1] S. T. Kumaravel, A. Murugesan, A. Kumaravel, *Renew. Sustain. Energy Rev.*, 2016, **60**, 1678-1685.

[2] J. Mabroukia, M. A. Abbassi, B. Khiari, S. Jellali, M. Jeguirim, *C. R. Chim.*, 2022, **25**, 81-92.

[3] E. T. B. Al-Tikrity, A. B. Fadhil, K. K. Ibraheem, *Energy Sources A: Recovery Util. Environ. Eff.*, 2017, **39**, 649-656.

[4] A. B. Fadhil, H. M. Mohammed, *Transport*, 2018, **33**, 686-698.

[5] V. O. Santos, L. S. Queiroz, R. O. Araujo, F. C. Ribeiro, M. N. Guimarães, C. E. da Costa, J. S. Chaar, L. K. de Souza, *Pyrolysis of acai seed biomass*, 2020, **12**, article no. 100553.

[6] H. Hammani, M. El Achaby, K. El Harfi, M. A. El Mhammedi, A. Aboulkas, *C. R. Chim.*, 2020, **23**, 589-606.

[7] J. Y. Jeong, C. W. Yang, U. D. Lee, S. H. Jeong, *J. Anal. Appl. Pyrol.*, 2020, **145**, article no. 104708.

[8] R. K. Mishra, R. Vinu, *J. Anal. Appl. Pyrol.*, 2024, **179**, article no. 106514.

[9] S. Kordoghli, E. Fassatoui, J. F. Largeau, B. Khiari, *C. R. Chim.*, 2023, **26**, 37-51.

[10] H. T. Tan, Z. Helwani, A. D. Wiheeb, J. Kim, M. R. Othman, *Energy Sources A: Recovery Util. Environ. Eff.*, 2015, **37**, 2437-2442.

[11] S. C. Patra, M. Vijay, A. K. Panda, *Int. J. Ambient Energy*, 2017, **38**, 788-793.

[12] R. K. Mishra, K. Mohanty, *Fuel*, 2020, **280**, article no. 118594.

[13] R. Kaur, V. T. Kumar, B. B. Krishna, T. Bhaskar, *Bioresour. Technol.*, 2023, **376**, article no. 128859.

[14] S. Y. Ibrahim, S. F. Mahmood, S. A. Younis, A. B. Fadhil, *Chem. Biodiversity*, 2023, **20**, article no. e202300103.

[15] M. A. Sokoto, B. Biswas, J. Kumar, T. Bhaskar, *Renew. Energy*, 2020, **146**, 1710-1716.

[16] A. M. Daabo, L. I. Saeed, M. H. Altamer, A. B. Fadhil, T. Badawy, *Renew. Energy*, 2022, **201**, 21-34.

[17] M. M. Hasan, M. G. Rasul, N. Ashwath, M. M. K. Khan, M. I. Jahirul, *Renew. Energy*, 2022, **194**, 1098-1109.

[18] A. Tabal, O. Belyazid, H. Dahman, E. Berrich, M. Jeguirim, M. El Achaby, K. El Harfi, A. Aboulkas, *C. R. Chim.*, 2023, **26**, 7-23.

[19] L. A. Saleh, N. M. T. Al-Layla, S. K. Saeed, M. H. Altamer, A. B. Fadhil, *Chem. Eng. Technol.*, 2024, **47**, 638-648.

[20] Y. Sun, C. Li, Q. Li, S. Zhang, L. Xu, M. Gholizadeh, X. Hu, *J. Energy Inst.*, 2021, **97**, 1-12.

[21] N. Ayrilmis, U. Buyuksari, E. Avci, E. Koc, *For. Ecol. Manage.*, 2009, **259**, 65-70.

[22] H. S. Altundoğan, A. Topdemir, M. Çakmak, N. Bahar, *J. Taiwan Inst. Chem. Eng.*, 2016, **58**, 219-225.

[23] M. S. S. Abujazar, S. U. Karaağaç, H. Ramadan, S. S. Abu Amr, M. Y. D. Alazaiza, *Desalin. Water Treat.*, 2022, **269**, 57-64.

[24] H. Guo, Y. Isoda, T. Honma, F. Shen, R. L. Smith Jr, *Renew. Energy*, 2024, **232**, article no. 121145.

[25] H. S. A. Turgut, I. Dincer, *Energy Convers. Manage.*, 2024, **310**, article no. 118474.

[26] R. Gurav, S. K. Bhatia, T. R. Choi, H. J. Kim, Y. K. Choi, H. J. Lee, Y. H. Yang, *Chemosphere*, 2022, **296**, article no. 134034.

[27] B. A. Khan, M. Ahmad, S. Iqbal, N. Bolan, S. Zubair, M. A. Shafique, A. Shah, *Environ. Res.*, 2022, **212**, article no. 113540.

[28] H. Xiong, Y. Xiao, Z. Yan, *Colloid Interface Sci. Commun.*, 2021, **43**, article no. 100460.

[29] S. Katiyar, R. Katiyar, *Biocatal. Agric. Biotechnol.*, 2024, **60**, article no. 103286.

[30] L. Ma, Y. Du, S. Chen, D. Du, H. Ye, T. C. Zhan, *Chemosphere*, 2022, **287**, article no. 132184.

[31] M. J. Saif, K. M. Zia, Fazal-Ur-Rehman, M. Usman, I. H. Abdullah, S. A. S. Chatha, *Water Environ. Res.*, 2015, **87**, 291-297.

[32] M. Masuku, J. F. Nure, H. I. Atagan, N. Hlongwa, T. T. I. Nkambule, *Sci. Total Environ.*, 2024, **908**, article no. 168136.

[33] G. M. Ayoub, A. Damaj, H. El-Rassy, M. Mahmoud Al-Hindi, R. M. Zayyat, *SN Appl. Sci.*, 2019, **1**, article no. 1562.

[34] P. McNamee, P. W. R. Adams, M. C. McManus, B. Dooley, L. I.

Darvell, A. Williams, J. M. Jones, *Energy Convers. Manage.*, 2016, **113**, 177-188.
[35] H. Kang, X. Guo, M. An, Q. Guo, G. Chang, *J. Anal. Appl. Pyrol.*, 2023, **172**, article no. 106022.
[36] Y. Chen, L. Wang, M. Zhao, H. Ma, D. Chen, Y. Zhang, J. Zhou, *ACS Omega*, 2021, **6**, 3490-3498.
[37] P. A. Bhavsar, M. H. Jagadale, Y. P. Khandetod, A. G. Mohod, *Int. J. Current Microbiol. Appl. Sci.*, 2018, **7**, 2846-2849.
[38] Y. Kar, *Biomass Bioenergy*, 2011, **35**, 4297-4304.
[39] A. M. Mansor, J. S. Lima, F. N. Anib, H. Hashima, W. S. Hoa, *Chem. Eng.*, 2019, **72**, 79-84.
[40] N. M. Al-Layla, L. A. Saleh, A. B. Fadhil, *J. Anal. Appl. Pyrol.*, 2021, **156**, article no. 105088.
[41] R. K. Mishra, V. Kumar, K. Mohanty, *J. Energy Inst.*, 2020, **93**, 1148-1162.
[42] A. S. Ibrahim, A. B. Fadhil, *J. Ecol. Eng.*, 2023, **24**, 225-241.
[43] W. Wu, C. Wu, G. Zhang, J. Liu, Y. Li, G. Li, *Fuel*, 2023, **332**, article no. 126107.
[44] R. A. Hasan, A. B. Fadhil, *Fuller Nanotub Car N*, 2023, **31**, 423-434.
[45] G. Zhang, H. Yang, M. Jiang, Q. Zhang, *Physicochem. Eng. Aspects*, 2022, **641**, article no. 128124.
[46] R. K. Mishra, K. Mohanty, *J. Anal. Appl. Pyrol.*, 2018, **134**, 83-92.
[47] S. Khalili, B. Khoshandam, M. Jahanshahi, *RSC Adv.*, 2015, **5**, 94115-94129.
[48] J. Wu, L. Wang, H. Ma, J. Zhou, *RSC Adv.*, 2021, **11**, 34795-34805.
[49] I. Neme, G. Gonf, C. Masi, *Results Mater.*, 2022, **15**, article no. 100304.
[50] M. S. Ahmad, M. A. Mehmood, O. S. Al Ayed, G. Ye, H. Luo, M. Ibrahim, G. Qadir, *Bioresour. Technol.*, 2017, **224**, 708-713.
[51] N. Agnihotri, M. K. Mondal, *J. Anal. Appl. Pyrol.*, 2023, **172**, article no. 106006.
[52] A. Nawaz, B. Singh, P. Kumar, *Indian J. Chem. Technol.*, 2021, **28**, 684-692.
[53] S. L. Narnaware, N. L. Panwar, *Bioresour. Technol. Rep.*, 2022, **17**, article no. 100942.
[54] K. Açıkalın, *Bioresour. Technol.*, 2021, **337**, article no. 125438.
[55] A. Sahoo, S. Kumar, J. Kumar, T. Bhaskar, *Bioresour. Technol.*, 2021, **319**, article no. 124060.
[56] H. Yang, R. Yan, H. Chen, D. H. Lee, C. Zheng, *Fuel*, 2007, **86**, 1781-1788.
[57] J. Shen, G. Huang, C. An, X. Xin, C. Huang, S. Rosendahl, *Bioresour. Technol.*, 2018, **247**, 812-820.
[58] Y. Chen, L. Wang, M. Zhao, H. Ma, D. Chen, Y. Zhang, J. Zhou, *ACS Omega*, 2021, **6**, 3490-3498.
[59] M. Boutaieb, M. Guiz, S. Román, S. Nogales, B. Ledesm, A. Ouederni, *Environ. Prog. Sustain. Energy*, 2019, **39**, article no. e13272.
[60] R. Garg, N. Anand, D. Kumar, *Renew. Energy*, 2016, **96**, 167-171.
[61] D. Pradhan, R. K. Singh, H. Bendu, R. Mund, *Energy Conversion Manage.*, 2016, **108**, 529-538.
[62] I. Demiral, N. G. Atilgan, S. Şensöz, *Chem. Eng. Commun.*, 2008, **196**, 104-115.
[63] S. Keleş, T. Kar, M. Akgün, K. Kaygusuz, *Energy Sources A: Recovery Util. Environ. Eff.*, 2017, **39**, 2216-2225.
[64] S. Chutiaa, R. Narzaria, N. Bordoloia, R. Saikiaa, L. Gogoia, D. Suta, N. Bhuyana, R. Katakia, *Mater. Today: Proc.*, 2018, **5**, 23193-23202.
[65] N. Khuenkaeo, S. Phromphithak, T. Onsree, S. R. Naqvi, N. Tippayawo, *PLoS One*, 2021, **16**, article no. e0254485.
[66] A. Aboulkas, H. Hammani, M. El Achaby, E. Bilal, A. Barakat, K. El Harfi, *Bioresour. Technol.*, 2017, **243**, 400-408.
[67] S. Suttibak, C. Saengmanee, A. Chuntanapum, *Heliyon*, 2024, **10**, article no. e28310.
[68] R. Sultana, U. Banik, P. K. Nandy, M. Nurul Huda, M. Ismail, *Energy Convers. Manage.: X*, 2023, **20**, article no. 100429.
[69] J. Jeong, H. W. Lee, S. H. Jang *et al.*, *Catalysts*, 2019, **9**, article no. 1034.
[70] V. Fierro, V. T. Fernfindez, A. Celzard, *Stud. Surf. Sci. Catal.*, 2007, **160**, 607-614.
[71] R. H. Al-Hyali, W. A. Alqazzaz, D. H. Altamer, *J. Turkish Chem. Soc. A: Chem.*, 2023, **10**, 339-358.
[72] M. C. da Silva, C. Schnorr, S. F. Lütke, S. Knani, V. X. Nascimento, É. C. Lima, G. L. Dotto, *Chem. Eng. Res. Des.*, 2022, **187**, 387-396.
[73] R. Y. Khalid, A. B. Fadhil, *Asia-Pac. J. Chem. Eng.*, 2024, **19**, article no. e2976.
[74] G. Duman, Y. Onal, C. Okutucu, S. Onen, J. Yanik, *Energy Fuels*, 2009, **23**, 2197-2204.
[75] D. H. Altamer, D. N. Saad, A. N. Al-Irhayim, A. B. Fadhil, *Int. J. Environ. Anal. Chem.*, 2024, 1-24.
[76] H. M. Jang, S. Yoo, Y. K. Choi, S. Park, E. Kan, *Bioresour. Technol.*, 2018, **259**, 24-31.
[77] W. Hu, X. Zhang, M. Chen, S. T. Rahman, X. Li, G. Wang, *Molecules*, 2024, **29**, article no. 2220.
[78] M. Jain, V. K. Garg, K. Kadirvelu, *J. Hazard. Mater.*, 2009, **171**, 328-334.
[79] A. Monika Jain, V. K. Garga, K. Kadirvelu, *Bioremed. J.*, 2013, **17**, 30-39.
[80] Z. Al-Qodah, R. Dweiri, M. Khader, S. Al-Sabbagh, M. Al-Shannag, S. Qasrawi, M. Al-Halawani, *Case Stud. Chem. Environ. Eng.*, 2023, **7**, article no. 100333.
[81] S. Amornwutiroj, P. Manpetch, W. Singhapong, P. Srinophakun, A. Jaroenworaluck, *J. Dispersion Sci. Technol.*, 2020, **41**, 1427-1444.
[82] F. Khemmari, K. Benrachedi, *Energy Sources A: Recovery Util. Environ. Eff.*, 2020, **42**, 688-699.
[83] M. K. Rai, G. Shahi, V. Meena, R. Meena, S. Chakraborty, R. S. Singh, B. N. Rai, *Resource-Efficient Technol.*, 2016, **2**, S63-S70.
[84] A. Kumar, H. M. Jena, *Process Saf. Environ. Prot.*, 2017, **109**, 63-71.
[85] H. N. Saeed, A. B. Fadhil, O. A. Shareef, *J. Ecol. Eng.*, 2024, **25**, 38-52.
[86] M. Kebir, R. Bourzami, N. Nasrallah *et al.*, *C. R. Chim.*, 2022, **25**, 9-25.
[87] K. Mahmoudi, N. Hamdi, M. Ben Ali, S. Jellali, E. Srasr, *C. R. Chim.*, 2020, **23**, 689-704.
[88] S. Jmai, S. Guiza, S. Jellali, M. Bagane, M. Jeguirim, *C. R. Chim.*, 2022, **25**, 27-41.
[89] A. Mlayah, S. Jellali, A. Azzaz, M. Jeguirim, H. Sellalmi, N. Hamdi, *C. R. Chim.*, 2021, **24**, 7-22.
[90] D. H. Altamer, W. A. Alqazzaz, A. B. Fadhil, *Iran. J. Chem. Chem. Eng.*, 2023, **42**, 139-154.